ADVANCED ENERGY MATERIALS
www.advenergymat.de

Strain-Induced Orbital Contributions to Oxygen Electrocatalysis in Transition-Metal Perovskites

*Abel Fernandez, Lucas Caretta, Sujit Das, Christoph Klewe, Djamila Lou, Eric Parsonnet, Ran Gao, Aileen Luo, Padraic Shafer, and Lane W. Martin**

Epitaxial strain has been shown to produce dramatic changes to the orbital structure in transition metal perovskite oxides and, in turn, the rate of oxygen electrocatalysis therein. Here, epitaxial strain is used to investigate the relationship between surface electronic structure and oxygen electrocatalysis in prototypical fuel cell cathode systems. Combining high-temperature electrical-conductivity-relaxation studies and synchrotron-based X-ray absorption spectroscopy studies of $La_{0.5}Sr_{0.5}CoO_3$ and $La_{0.8}Sr_{0.2}Co_{0.2}Fe_{0.8}O_3$ thin films under varying degrees of epitaxial strain reveals a strong correlation between orbital structure and catalysis rates. In both systems, films under biaxial tensile strain simultaneously exhibit the fastest reaction kinetics and lowest electron occupation in the d_{z^2} orbitals. These results are discussed in the context of broader chemical trends and electronic descriptors are proposed for oxygen electrocatalysis in transition metal perovskite oxides.

1. Introduction

Transition metal perovskite oxides represent a critical component in solid oxide fuel cells and solid oxide electrolyzer cells. In these ABO_3 perovskites, the transition metal at the *B* site serves as the catalytically active site in the oxygen-reduction reaction (ORR), converting molecular oxygen to lattice oxygen, or vice versa in the oxygen-evolution reaction (OER). Perovskites with iron, cobalt, manganese, and/or nickel cations at the *B* site have shown high activities and represent a cost-effective alternative to expensive noble metal-based catalysts; however, gas exchange at these perovskite surfaces remains the limiting factor for high efficiency in electrochemical devices.[1–3]

The development of perovskites with high activity has historically relied on brute-force compositional screening involving the synthesis and testing of numerous bulk-ceramic samples to establish an intuition for chemical trends that can guide researchers to highly active compositions. More recently, however, there has been a significant push to develop electronic descriptors for predicting electrochemical activity.[4–7] This work has led to the identification of several electronic descriptors that are closely correlated with high activity for ORR and OER catalysts, including the relative position of the oxygen 2*p* band center,[6] the *B*—O bond covalency,[8] and, in particular, the occupancy of the e_g orbitals.[5,9] For example, e_g orbital occupation has been shown to be strongly correlated with the *B*-site-dependent chemical activity trends, and an "ideal" e_g occupancy of ≈1.2 electrons has been used as the justification for high activities in $LaNiO_3$ and $Ba_{0.5}Sr_{0.5}Co_{0.8}Fe_{0.2}O_{3-\delta}$ (BSCF) catalysts.[5,9,10] As such, the development of electronic descriptors has already proved fruitful in identifying compositions with high activities and, in turn, developing synthetic control of materials properties to tune the electronic structure toward these ideal values could unlock a new way to optimize materials.

In parallel to the development of these electronic descriptors, researchers have leveraged thin-film-based studies to understand how manipulation of the lattice structure of these perovskites can affect the electrochemical activity. Several studies have focused on the role of epitaxial strain in perovskite oxides for controlling electrochemical activity.[11–17] Reports have noted enhanced electrochemical activities in cobalt- and iron-based perovskites under biaxial-tensile strain driven by strain-induced changes to surface chemistry[12] or suggested electronic contributions as the driving force for enhanced electrochemical activity under tensile strain.[13,14,18] Meanwhile, strain-induced changes to e_g occupancy have been proposed as the mechanism of enhanced ORR/OER activities in $LaNiO_3$ films under biaxial compressive strain.[16] This discrepancy suggests that strain-induced changes to electronic structure may be dependent on the identity of the *B*-site cation and calls for more direct studies

A. Fernandez, L. Caretta, S. Das, D. Lou, E. Parsonnet, R. Gao, A. Luo, L. W. Martin
Department of Materials Science and Engineering
University of California
Berkeley, CA 94720, USA
E-mail: lwmartin@berkeley.edu

A. Fernandez, L. Caretta, S. Das, D. Lou, E. Parsonnet, R. Gao, A. Luo, L. W. Martin
Materials Sciences Division
Lawrence Berkeley National Laboratory
Berkeley, CA 94720, USA

C. Klewe, P. Shafer
Advanced Light Source
Lawrence Berkeley National Laboratory
Berkeley, CA 94720, USA

The ORCID identification number(s) for the author(s) of this article can be found under https://doi.org/10.1002/aenm.202102175.

DOI: 10.1002/aenm.202102175

of the effect of strain on electronic structure in these perovskite catalysts.

Here, we examine the interplay between epitaxial strain, orbital structure, and electrochemical activity in two prototypical catalyst systems. Utilizing epitaxial strain imposed by various substrates in thin films of $La_{0.5}Sr_{0.5}CoO_3$ (LSCO) and $La_{0.8}Sr_{0.2}Co_{0.2}Fe_{0.8}O_3$ (LSCF), we correlate high-temperature electrochemical measurements with the structure of the catalytically active transition-metal sites. In both cases, biaxial tensile strain enhances the reaction rates for oxygen exchange, in agreement with previous studies on similar compositions. We additionally study the strain-induced changes to the electronic structure using X-ray linear dichroism measurements at the iron- and cobalt-*L* edges. It is shown that the biaxial strain and associated symmetry breaking of the oxygen octahedra shifts the energy levels of the two transition-metal e_g orbitals with respect to one another, ultimately changing the occupancy of the d_z^2 orbital. Together, electrochemical and absorption measurements point to a strong correlation between exchange rates and d_z^2 occupancy, with fast exchange rates found in films with lower d_z^2 occupancy. We propose, therefore, that the d_z^2 orbital is the key orbital involved in oxygen interaction at the perovskite surface and is responsible for strain-induced changes to electrocatalytic activity. These results advance the understanding of the role of the electronic structure in oxygen electrocatalysis, provide a mechanism to enhance chemical activity of oxygen electrocatalysis in thin films, and provide an explanation for several previously reported results regarding epitaxial strain-dependent electrochemical activities.

2. Results and Discussion

2.1. Synthesis and Characterization

Two sample variants were examined in this study. First, we studied 20-nm-thick films of LSCO deposited on the $LaAlO_3$ (001), $(LaAlO_3)_{0.3}(Sr_2TaAlO_6)_{0.7}$ (LSAT) (001), and $SrTiO_3$ (001) substrates, corresponding to biaxial strains of –1.22%, 0.87%, and 1.79%, respectively, imposed on the LSCO; henceforth referred to as LSCO/$LaAlO_3$ (–1.22%), LSCO/LSAT (+0.87%), and LSCO/$SrTiO_3$ (+1.79%) heterostructures. Second, we studied 20-nm-thick films of LSCF deposited on LSAT (001), $SrTiO_3$ (001), and $DyScO_3$ (110) substrates, corresponding to biaxial strains of –0.97%, –0.02%, and 1.09%, respectively,[19,20] imposed on the LSCF; henceforth referred to as LSCF/LSAT (–0.97%), LSCF/$SrTiO_3$ (–0.02%), and LSCF/$DyScO_3$ (+1.09%) heterostructures. All films were grown via pulsed-laser deposition (Experimental Section).[20] Following film growth, X-ray diffraction studies (Experimental Section) were carried out to characterize the resulting structures and strain states (**Figure 1**). The systematic decrease in the out-of-plane *c* lattice parameter with increasing tensile strain is apparent in both the LSCO and LSCF films as a progressive shift of the 002-diffraction condition to higher 2θ angles (Figure 1a,b). Additionally, reciprocal space mapping (RSM) studies about the 103-diffraction condition were performed to examine the in-plane lattice parameters and reveal that all films are coherently strained to the substrate (Figure 1c–h). The surfaces of the as-grown films were characterized with atomic force microscopy (AFM, Experimental Section), and it was found that all films exhibit smooth surfaces with root-mean square roughness $\lesssim$1 nm (Figure S1, Supporting Information). Additionally, considering reports of strain-induced changes to surface strontium segregation, we studied the surface chemistry of the LSCF films, but found minimal differences to the surface chemistry in the as-grown state (Experimental Section and Figure S1, Supporting Information). Overall, high-quality thin films of both LSCO and LSCF were produced in three different strain states, providing a model set of samples in which to probe the connection between electrochemical reactivity and electronic structure.

2.2. Electrical Conductivity Relaxation

The oxygen exchange rates of the films were measured via the electrical-conductivity-relaxation (ECR) method at 300 °C (Experimental Section) whereby the resistance of the films was measured as a function of time following a step-change in the oxygen-partial pressure. The defect equilibria of these materials dictate that upon decreasing (increasing) the partial pressure of oxygen (p_{O2}) surrounding the films, the lattice will release (incorporate) oxygen to the environment (film), ultimately reducing (increasing) the conductivity of the films until it reaches a new equilibrium.[21] The ECR measurement is a commonly used technique for determining the oxygen-exchange and bulk-diffusion coefficients[12,21–25] In thin films, however, the small sample dimensions mean that the changes to conductivity are dominated by the surface reaction, allowing for direct comparison of the oxygen-exchange rates of the perovskite surfaces. ECR curves measured on strained LSCO films show an increase in resistance following a sudden drop in p_{O2} from 1 atm to 0.2 atm (**Figure 2**a and Figure S2, Supporting Information). It is observed that the highly compressively strained LSCO/$LaAlO_3$ (–1.22%) heterostructures take the longest to equilibrate (approaching 30 min for full equilibration), whereas the tensile strained LSCO/LSAT (+0.87%) and LSCO/$SrTiO_3$ (+1.79%) heterostructures equilibrate in just 3–10 min. Fitting the rate of change of the normalized resistance to the following expression provides for extraction of a surface-reaction rate constant,[26]

$$\frac{R_t - R_0}{R_\infty - R_0} = 1 - \exp\left(\frac{k_s}{d} * t\right) \quad (1)$$

where *t* is the time measured after the pressure change, *d* is the film thickness, and R_0, R_t, and R_∞ are the measured resistances before the pressure change, at time *t*, and after the film has equilibrated to a new value, respectively. Fitting each curve to this equation, we extract the surface-reaction rate constant, k_s for all strain states. The extracted rate constants for LSCO/$SrTiO_3$ (+1.79%), LSCO/LSAT (+0.87%), and LSCF/$LaAlO_3$ (–1.22%) heterostructures are 2.8×10^{-8}, 1.1×10^{-8}, and 1.5×10^{-9} cm s^{-1}, respectively, demonstrating an order of magnitude enhancement for films under large tensile strain compared to the films under large compressive strain (Figure 2a, inset). This difference is similar in magnitude to previously reported strain-induced changes.[12] A similar trend for strained LSCF films

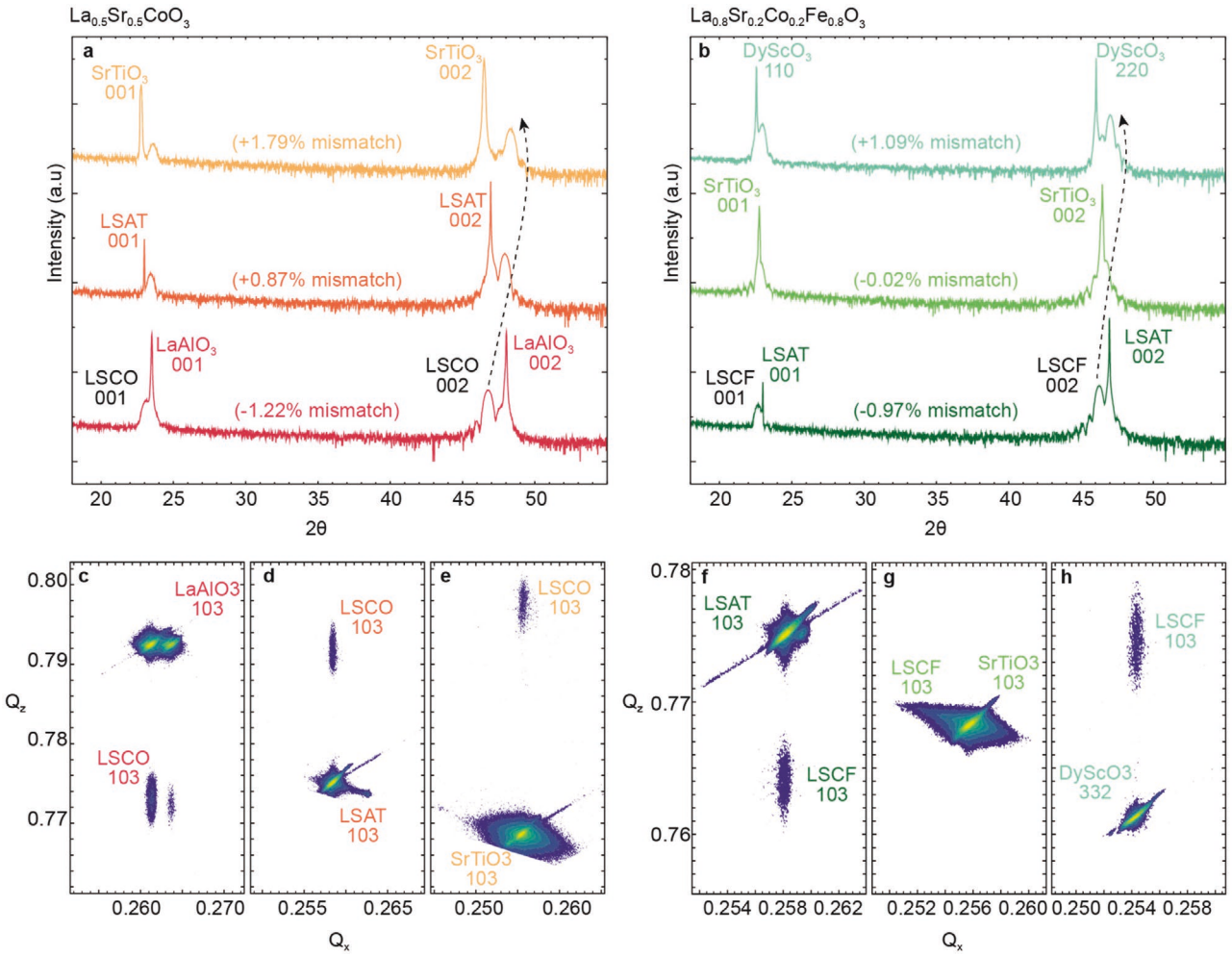

Figure 1. Structural characterization of LSCO and LSCF thin films. θ–2θ line scans for a) LSCO and b) LSCF thin films, on various substrates illustrate the decreasing c lattice parameter (increasing 2θ) for increasing tensile strain in all cases. Reciprocal space maps (RSMs) about the 103-diffraction conditions of c–e) LSCO and f–h) LSCF thin films demonstrate the high-quality epitaxial thin films are coherently strained to the substrate in all cases.

is observed; namely, close to an order of magnitude increase in rate constant in films under tensile strain (on $DyScO_3$ substrates) as compared to those under compressive strain (on LSAT substrates) (Figure 2b and inset). While the poor thermomechanical stability of LSCO prevented more extensive temperature-dependent studies,[2,27] we performed additional measurements on the LSCF heterostructures at 275 and 325 °C (Figure 2c). Temperature-dependent ECR was measured for both heating (i.e., measuring first at 275 °C and increasing the temperature thereafter) as well as cooling (i.e., measuring first at 325 °C and decreasing the temperature thereafter) with no significant difference observed between the routines, suggesting that sample aging did not play an important role in the temperature-dependence observed. LSCF/$DyScO_3$ (+1.09%) heterostructures maintained the fastest surface reaction rate over the temperature range studied, while the LSCF/LSAT (–0.97%) heterostructures remained the slowest. Fitting the temperature-dependence of the rate constants for the LSCF films showed small differences in activation energy E_a, between 0.50–0.66 eV, similar to activation energies reported for other iron-based cathodes and suggesting that any strain-induced difference in E_a is within the error of the measurement and, therefore, does not provide sufficient explanation as to the differences between rate constants (Figure 2c, inset). Overall, these results establish that epitaxial strain can induce changes to oxygen-exchange rates. In agreement with previous reports on cobalt and iron-based cathodes, biaxial-tensile strain is shown to increase reaction rates, while biaxial-compressive strain reduces reaction rates. Now, we turn to a study of the electronic structure to ascertain whether strain-induced changes to the orbital structure could be driving the electrochemical differences.

2.3. X-ray Absorption and Linear Dichroism

To probe strain-induced changes to the surface electronic structure, we performed X-ray absorption and linear dichroism studies on the epitaxially strained LSCO and LSCF films at beamline 4.0.2 at the Advanced Light Source, Lawrence Berkeley National Laboratory (Experimental Section). Here, the absorption is measured with photons polarized parallel to the plane of the thin film ($E//ab$) as well as nearly perpendicular to

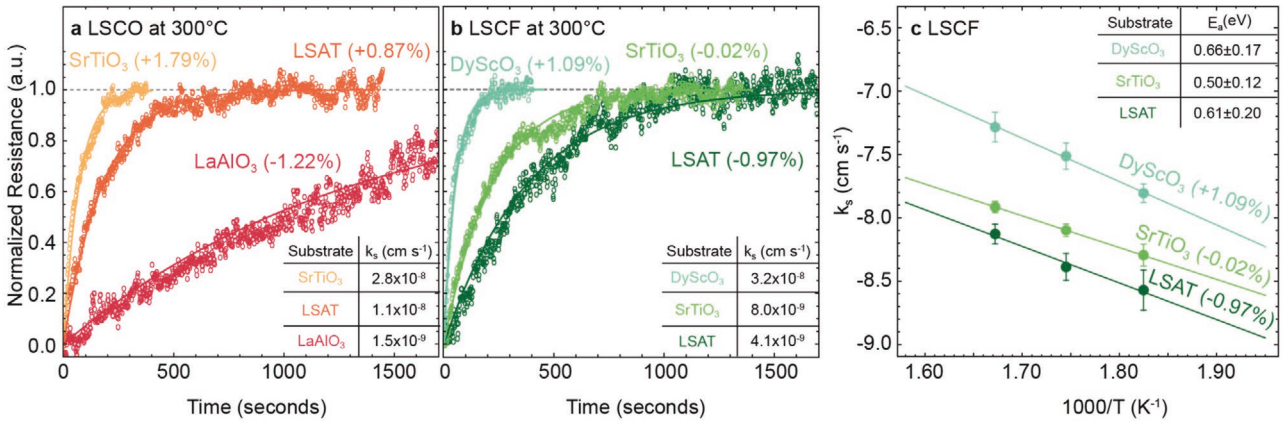

Figure 2. Electrochemical testing of a) LSCO thin films on various substrates at 300 °C showing the fastest relaxation kinetics for films deposited on $SrTiO_3$ (001) substrates, corresponding to +1.79% tensile strain. Inset table shows extracted rate constants, k_s, for each strain state. b) Measurements on LSCF thin films at 300 °C showing a similar trend, with films under tensile strain having faster reaction kinetics than the low- or compressively strained films on $SrTiO_3$ and LSAT substrates, respectively. Inset table shows the extracted rate constants, k_s, from each strain state. c) The strain-dependence of the reactions rates for the LSCF thin films holds over a range of temperatures. Inset shows the extracted slopes of the temperature-dependence and that each strain state gives rise to a comparable activation energy.

the plane of the film ($E//c$) (**Figure 3**a). XLD is defined as the difference between the spectra measured with $E//ab$ and $E//c$ (i.e., $I_{ab} - I_c$). Larger absorption from $E//ab$ (i.e., $I_{ab} - I_c > 0$) indicates more empty in-plane states, whereas larger absorption from $E//c$ (i.e., $I_{ab} - I_c < 0$) indicates more empty out-of-plane states. Moreover, absorption is measured via a total electron yield (TEY) process, ensuring that the studies are sensitive to only the top few nanometers of the film, thus probing the portion of the film most directly exposed to the environmental gas and involved in oxygen electrocatalysis.

First, we examined the cobalt-L edge for strained LSCO heterostructures (Figure 3b and Figure S3a–c, Supporting Information). The relatively broad L_3 and L_2 peaks confirm a mixture of Co^{3+} and Co^{4+} that is caused by the aliovalent doping of Sr^{2+} on the La^{3+} site.[28] Moreover, there has been significant discussion regarding the spin state in Co^{3+}-based perovskites, with competition between high-spin (HS, $t_{2g}^4e_g^2$), low-spin (LS, $t_{2g}^6e_g^0$), and intermediate-spin (IS, $t_{2g}^5e_g^1$) states which are relatively close in energy with each producing unique X-ray absorption and XLD spectra.[28–30] In the $La_{1-x}Sr_xCoO_{3-\delta}$ system, spectroscopic studies have proposed that the cobalt exists predominantly as a mixture of HS Co^{3+}, and HS Co^{4+}, with some LS Co^{3+} that decreases in prevalence with increasing Sr^{2+} content.[28] The spectra observed here are consistent with the presence of HS Co^{3+} and Co^{4+} and the relatively high Sr^{2+} content (50%) and suggests that the fraction of LS Co^{3+} is likely to be low in these samples; thus we assume a HS configuration for further analyses (see Supporting Information for further discussion). In this case, the significant filling of the t_{2g} orbitals suggests that the majority of the electronic changes observed will originate in the e_g orbitals. We indeed see differences in the absorption of in-plane ($E//ab$) and out-of-plane ($E//c$) X-rays mainly occurring on the high-energy side of the L_3 and L_2 edges, suggesting epitaxial strain is primarily modulating the electron occupancy of the e_g orbitals in LSCO. The strain-induced changes are best observed in the linear dichroism. For LSCO/$LaAlO_3$ (–1.22%) heterostructures under biaxial compressive strain (Figure 3b), the integrated area is largely positive, indicating more empty in-plane states, whereas for the LSCO/LSAT (+0.87%; Figure 3c) and LSCO/$SrTiO_3$ (+1.79%; Figure 3d) heterostructures under tensile strain we see the inverse, with large negative areas, indicating more empty out-of-plane states.

In the case of the iron-L edge in the LSCF films, the spectra generally resemble that of $LaFeO_3$, characterized by doublets in both the L_3 and L_2 edges (Figure 3e–g and Figure S3c–e, Supporting Information), indicating the iron is primarily in the Fe^{3+} state.[8,31] Examining the L_3 edge, the strongest peaks, centered around 709.5 eV, correspond to the e_g states, while the smaller peak at lower energies corresponds to the t_{2g} states. Beginning with the low-strain LSCF/$SrTiO_3$ (–0.02%) heterostructure, the spectra measured with in- and out-of-plane polarized X-rays are almost identical, exhibiting near-zero dichroism, as expected for a cubic perovskite (Figure 3f). Applying strain, however, results in the emergence of more significant dichroism with the LSCF/LSAT (–0.97%; Figure 3e) and LSCF/$DyScO_3$ (+1.09%; Figure 3g) heterostructures showing inverted dichroism relative to one another. This inversion of the difference curve is an indication of inversion of the preferential occupation of the orbitals. Despite the linear dichroism for strained LSCF heterostructures showing a more complex shape, we expect the epitaxial strain to primarily modulate the energies of the e_g orbitals, and measurements of the oxygen-K edge in LSCF supports this (Figure S4, Supporting Information). Thus, the same trend is observed for both LSCO and LSCF films: that the integrated area of the linear dichroism becomes increasingly negative as the films are subjected to increasing tensile strain (Figure 3h). This confirms that applying tensile strain results in an increase in the density of available states in the out-of-plane-oriented d orbitals for both LSCO and LSCF films.

To take a more quantitative approach to the analysis, we examined the energy splitting and electron occupation of the orbitals in question. It is understood that in many transition-metal perovskite oxides the conventional ligand-field model suggests that changing the overlap of the transition metal 3d

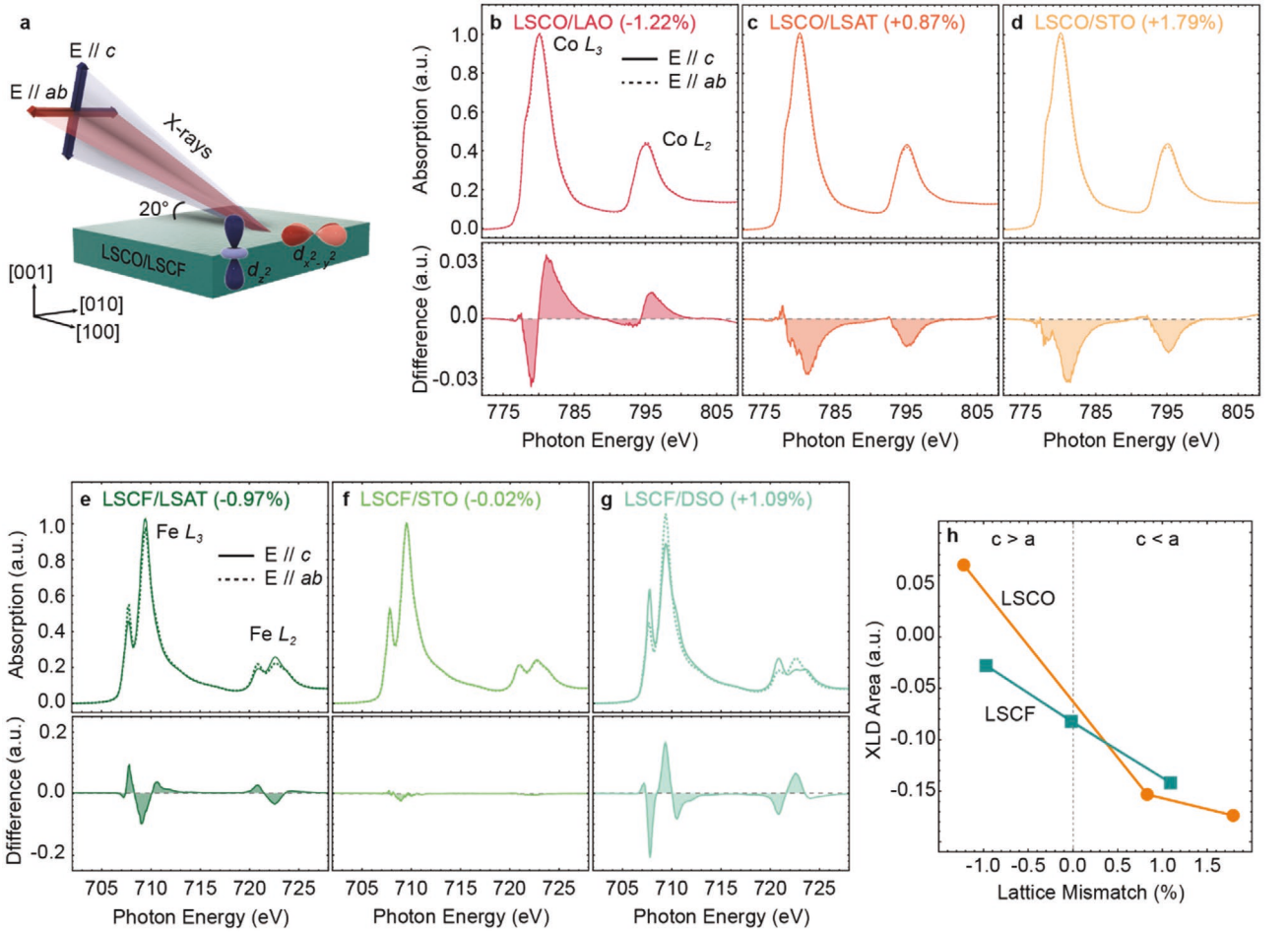

Figure 3. XLD measurements of LSCO and LSCF films. a) The grazing incidence geometry allows for selectively probing the difference between the in-plane $d_{x^2-y^2}$ (red) and out-of-plane d_{z^2} (blue) orbitals. b–d) Measurements of the cobalt-L edge show an inversion of the dichroism moving from compressive strain (LSCO/LAO) to tensile strain (LSCO/LSAT and LSCO/STO). e–g) XLD at the iron-L edge in LSCF films shows a similar inversion of the dichroism between compressive (LSCF/LSAT) and tensile (LSCF/DSO) strain states, while the low-strain, cubic film (LSCF/STO) shows no dichroism. h) The total integrated XLD area is summarized demonstrating that increasingly tensile strain (decreasing c/a ratio) results in more negative XLD area, corresponding to more empty states oriented out-of-plane.

orbitals with the oxygen 2*p* orbitals shifts the energy of the electrons within these orbitals, with biaxial compressive strain increasing the energy of the $d_{x^2-y^2}$ orbital relative to the d_{z^2} and vice versa for biaxial tensile strain (**Figure 4**a).[32] In turn, we estimate the strain-induced energy splitting of the e_g orbitals by comparing the difference in energy of the L_3 peak for vertically and horizontally polarized light for the cobalt-*L* edge in LSCO (Figure 4b). The peak energy of the in-plane polarized light decreases by ≈100 meV, with increasing tensile strain, whereas the peak energy for the out-of-plane polarized light increases by ≈25 meV. To quantify the strain-induced energy difference between the e_g orbitals, we define:

$$\Delta e_g = E_{max}(E//ab) - E_{max}(E//c) \approx E\left(d_{x^2-y^2}\right) - E\left(d_{z^2}\right) \quad (2)$$

In both LSCO and LSCF, Δe_g goes from positive to negative as we move from compressive to tensile strain (Figure 4c). In a cubic crystal field, these two e_g orbitals are energetically degenerate, as evidenced by the smallest Δe_g for the LSCF/$SrTiO_3$ (–0.02%) heterostructures and, thus, electrons are more equally distributed between the two e_g orbitals. When biaxial strain is applied, however, the associated symmetry-breaking removes the energetic degeneracy and we see that under tensile strain $\Delta e_g < 0$ (i.e., the d_{z^2} orbital is higher in energy relative to the $d_{x^2-y^2}$ orbital) and under compressive strain $\Delta e_g > 0$ (i.e., the d_{z^2} orbital is lower in energy relative to the $d_{x^2-y^2}$ orbital). This breaking of the energetic degeneracy of the e_g orbitals is expected to also break the degeneracy in electron occupancy of the two e_g orbitals.[32–34] That is, electrons will preferentially occupy the lower-energy orbital, thereby reducing the occupancy of the higher-energy orbital. In this case, the reduction of the $d_{x^2-y^2}$ orbital energy under tensile strain results in preferential occupation of the lower-energy $d_{x^2-y^2}$ orbital and a reduction of the electron occupancy in the higher-energy d_{z^2} orbital. Using established sum rules for linear dichroism, we estimated this change in occupancy of the d_{z^2} orbital for each of the films under study (see Supporting Information for further discussion).[35–37] In the case of both sets of films, we see that the reduction in the energy of the $d_{x^2-y^2}$ orbital under increasing tensile strain results in a reduction of the d_{z^2}-orbital occupancy

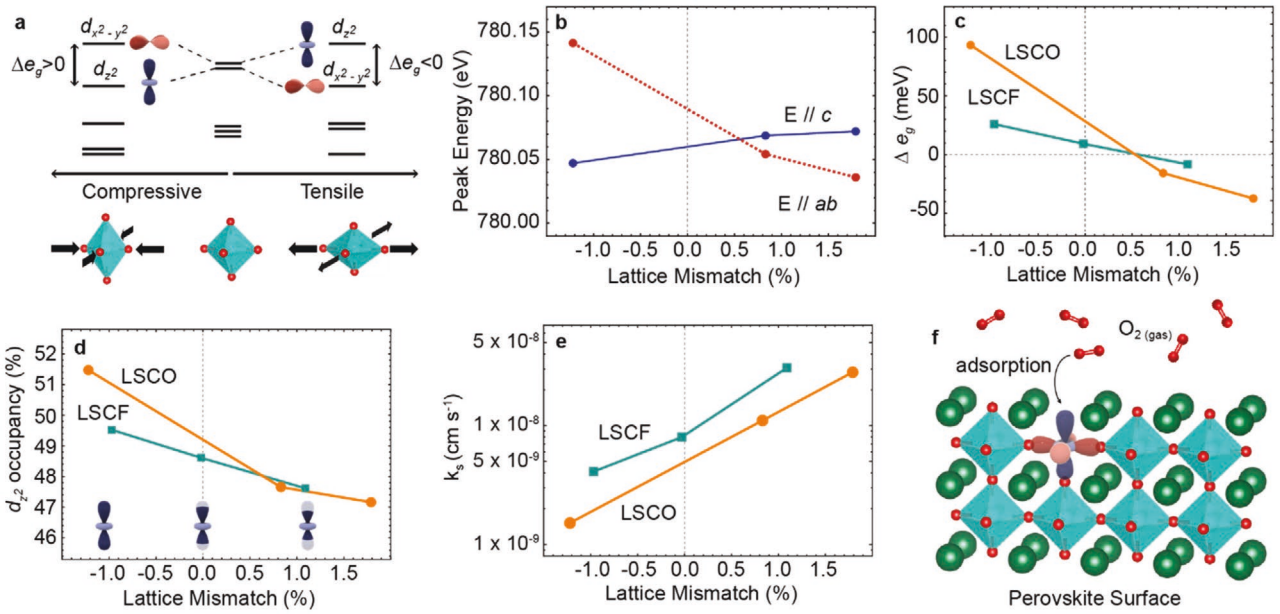

Figure 4. Orbital occupation and oxygen reactivity. a) Schematic illustrating the relationship between epitaxial strain and orbital energies in perovskite oxides showing that applying compressive strain breaks the e_g degeneracy and shifts the $d_{x^2-y^2}$ orbital higher in energy than the d_{z^2} orbital, while for tensile strain the $d_{x^2-y^2}$ orbital is lower in energy. b) Peak energies extracted from the cobalt-L edge in LSCO films demonstrate this trend, as the in-plane peak energy, corresponding to the $d_{x^2-y^2}$ orbital shifts lower in energy with tensile strain. c) The difference in orbital energy, Δe_g, changes sign moving from compressive to tensile strain, with LSCO demonstrating a larger strain-induced change in orbital energies than LSCF. d) Calculation of the strain-dependent occupancy of the d_{z^2} orbital shows that increasing tensile strain reduces the occupancy toward the proposed optimal value of ≈30% and this reduction in occupancy is correlated to the increase in reaction rates with strain summarized in (e). f) Schematic showing that the d_{z^2} orbital plays an important role in oxygen electrocatalysis as the primary orbital for interaction oxygen gas molecules adsorbing at the perovskite surface.

as electron density shifts from the $d_{x^2-y^2}$ orbital to the d_{z^2} orbital (Figure 4d). We note that the trends in orbital occupancy (calculated from the total integrated intensities of each spectrum) and the trends in Δe_g (calculated from peak energies) are in agreement for both compositions, albeit with different magnitudes for LSCO and LSCF, supporting the strain-induced Δe_g splitting as a driving force for changes to d_{z^2}-orbital occupancy. Overall, this demonstrates that epitaxial strain can be used to modulate the occupancy of the d_{z^2} orbitals.

2.4. Orbital Occupation and Electrocatalysis

We now turn our attention to the relationship between orbital structure and the electrochemical results reported here and elsewhere.[12–17] Recall that the rate constants in both LSCO and LSCF films increased monotonically as the strain state was changed from compressive to tensile, or in other words as the c/a lattice parameter ratio decreased (Figure 4e). Corresponding to this change in rate constant with strain, we observed an overall decrease in the electron occupancy of the d_{z^2} orbital with increasing tensile strain in both materials. The correlation here is further supported by measurements on LSCF/$TbScO_3$ (+1.23%) heterostructures (Figure S5, Supporting Information). In those heterostructures, despite larger lattice mismatch, both measured rate constants and the linear dichroism were decreased with respect to LSCF/$DyScO_3$ (+1.09%) heterostructures. As such, the measured linear dichroism and calculated orbital occupancy provides a stronger predictor for reaction rate constants than the epitaxial strain (see Supporting Information for further discussion). In the context of the proposed electronic descriptors, specifically the e_g filling, this strong correlation between d_{z^2}-orbital occupancy and rate constant is interesting because the overall e_g filling does not change with strain, only the relative occupation of the two non-degenerate orbitals has changed. The correlation to the occupancy of the d_{z^2} orbital can then be understood in that the d_{z^2} orbital is the orbital that is projected out of the surface of an [001]-oriented thin film, and would have the most orbital overlap with the oxygen 2*p* orbitals of the incoming oxygen molecule to be adsorbed at the transition metal *B* site (Figure 4f); a process which has been shown to be a critical step in the activation and incorporation of molecular oxygen at perovskite surfaces.[38] In this case, the ideal value is no longer an e_g filling of ≈1.2 electrons,[5] but instead would be ≈0.6 electrons in the d_{z^2} orbital, or ≈30% occupancy. As observed here, at the cobalt and iron sites in LSCO and LSCF, respectively, the d_{z^2}-orbital occupancy is near 50% at zero strain, and is decreased toward the optimal value of ≈30% with the application of tensile strain. The occupancy trends extracted from both the strained LSCO and LSCF films thus provide additional rationale for the observation of enhanced oxygen electrocatalysis in cobalt- and iron-based perovskites under epitaxial tensile strain reported previously.[12–14,17] Moreover, this insight may also explain the somewhat contradictory report of enhanced bifunctional catalysis of $LaNiO_3$ thin films under compressive strain.[16] Because of the robust low-spin $t_{2g}^6e_g^1$ electron configuration of the Ni^{3+} in those films, the zero-strain state likely has a d_{z^2} orbital occupancy of ≈25%, and thus compressive strain

increases the d_z^2 orbital occupancy towards the ideal value near ≈30%. This sort of chemistry dependence is evident even in the present work, where both the d_z^2-orbital occupancy and rate constant are more dramatically modulated by the application of epitaxial strain in the LSCO films as compared to the LSCF films. The robust, half-filled $t_{2g}^3 e_g^2$ electron configuration of the Fe^{3+} site in LSCF likely prevents more significant orbital polarization in the e_g levels, due to the electron-electron repulsion associated with trying to increase electron density in the already singly occupied $d_{x^2-y^2}$ orbital, whereas the more complex $Co^{3+/4+}$ system having HS $t_{2g}^4 e_g^2$, LS $t_{2g}^6 e_g^0$, and IS $t_{2g}^5 e_g^1$ states could allow for more flexibility by shifting electron density into the $d_{x^2-y^2}$ orbital since a larger fraction throughout the film may be empty. This dependence on chemistry suggests that the connection between epitaxial strain and oxygen electrocatalysis observed for cobalt- and iron-based perovskites in this and previous studies is not universal but is strongly dependent on the zero-strain electronic configuration.

3. Conclusion

In summary, we have demonstrated a strong correlation between the orbital structure and oxygen electrocatalysis rates in cobalt- and iron-based perovskite oxides. Electrochemical studies on epitaxially strained LSCO and LSCF thin films confirm an activity trend previously reported by several groups, namely that biaxial tensile strain enhances oxygen reactivity, while biaxial compressive strain suppresses oxygen reactivity. We find that an important descriptor for this activity trend for the LSCO and LSCF films is the electron occupancy of the d_z^2 orbital, which is directly involved in the surface reaction of these perovskites with molecular oxygen. In addition to identifying the d_z^2 orbital as the electrochemically active orbital in [001]-oriented thin films, this work also demonstrates that epitaxial strain can be used as a synthetic tool to modulate the electron occupancy of this orbital and subsequently enhance the reactivity of these perovskite catalysts.

4. Experimental Section

Synthesis of Epitaxial Thin Films: Thin films were synthesized via pulsed-laser deposition using a KrF excimer laser (248 nm; LPX 305, Coherent, Inc). 20-nm-thick LSCO films were deposited from a ceramic target (Praxair) of the same chemistry ($La_{0.5}Sr_{0.5}CoO_3$) on $LaAlO_3$ (001), LSAT (001), and $SrTiO_3$ (001) substrates (Crystec, GmBH) at a heater temperature of 700 °C in a dynamic oxygen pressure of 200 mTorr with a laser fluence of 1.0 J cm^{-2} at a repetition rate of 10 Hz. 20-nm-thick LSCF films were deposited from a ceramic target (Praxair) of the same chemistry ($La_{0.8}Sr_{0.2}Co_{0.2}Fe_{0.8}O_3$) on LSAT (001), $SrTiO_3$ (001), and $DyScO_3$ (110) substrates (Crystec, GmBH) at a heater temperature of 650 °C and a dynamic oxygen pressure of 200 mTorr using a laser fluence of 0.9 J cm^{-2} at a repetition rate of 5 Hz. Following deposition, all films were cooled in a static oxygen pressure of 700 Torr. LSCF films were cooled at a rate of 10 °C min^{-1} following deposition, whereas the LSCO films were cooled at a rate of 5 °C min^{-1} to avoid cracking the films.

Characterization of Crystal Structure and Surface Topography: X-ray studies were conducted with a high-resolution X-ray diffractometer (X'pert Pro^3, PANalytical) utilizing a PIXcel3D-Medipix3 detector. θ–2θ line scans were measured from 10–60° to probe the out-of-plane lattice-spacing of the films, utilizing line-detection mode. Two-dimensional reciprocal space maps were measured using the full-frame area detection of the PIXcel3D-Medipix3 detector. In the case of the cubic substrates (i.e., $LaAlO_3$, LSAT, and $SrTiO_3$), RSMs were completed about the 103-diffraction condition, whereas for orthorhombic substrates (i.e., $DyScO_3$), RSMs were centered about the 332-diffraction condition allowing for measurement of the films 103-diffraction condition in all cases. Surface topography was studied using an atomic force microscope (MFP-3D, Asylum Research).

Evolution of Surface Chemistry: Samples were annealed in a tube furnace at 350 °C in air using a 10 °C min^{-1} ramp rate for heating and cooling, with varying dwell times to study the evolution of surface chemistry under conditions similar to those in the ECR measurements. Following the annealing steps, the surface of each sample was characterized via X-ray photoelectron spectroscopy (XPS, PHI 5600) at a pressure <10^{-9} Torr using an aluminum K_α (1486.6 eV) source. Spectra for the strontium 3*d* excitation were fit using the CasaXPS software with a symmetric line shape and fixed branching ratio of 3:2. Following surface characterization, samples were returned to the furnace for the next anneal step (Figure S1, Supplemental Information).

Electrochemical Measurements: ECR measurements were carried out in a home-built, tube-furnace-based measurement system. Prior to measurement, 100 µm circular platinum contacts with 200 µm spacing were deposited. Contacts were wire-bonded to a CERDIP chip carrier with gold wire before mounting in the tube furnace. A Keithley 2400 was used to measure the 4-point resistance of the sample. A 7 µA drive current was used for LSCF films whereas a 700 µA drive current was used for LSCO films. A 1000 sccm gas flow was maintained for the duration of the electrochemical experiments, controlled by 2 mass flow controllers to ensure a fast pressure change in the tube. The partial pressure of oxygen was changed utilizing a 3-way valve to change the input of one mass flow controller between N_2 and O_2, while another mass flow controller continuously flowed O_2. In all cases, at least three films of each composition and strain state were measured to ensure results were repeatable.

X-ray Absorption and Linear Dichroism Spectroscopy: X-ray absorption spectra were measured on 20-nm-thick films deposited under identical conditions to those used for electrochemical measurements. Measurements were carried out at Beamline 4.0.2 of the Advanced Light Source, Lawrence Berkeley National Laboratory at room-temperature in total-electron-yield (TEY) mode. Grazing incidence measurements were performed at an incident angle of 20° with respect to the sample surface while normal incidence scans were performed with an incident angle of 90° with respect to the sample surface. The X-ray energy and polarization was selected using an elliptically polarizing undulator. The intensity of the incident X-ray beam and sample drain current were simultaneously measured to normalize the absorption intensity. The linear dichroism measurements were obtained from the difference of horizontal and vertical polarized X-ray absorption spectra.

Supporting Information

Supporting Information is available from the Wiley Online Library or from the author.

Acknowledgements

A.F. acknowledges the support of the National Science Foundation under Grant OISE-1545907 and the NSF GRFP. L.C. acknowledges financial support from the Ford Foundation and from the University of California Office of the President. S.D. acknowledges the Quantum Materials program of the Office of Basic Energy Sciences, U.S. Department of Energy. D.L. acknowledges the support of the Army Research Office under Grant W911NF-21-1-0118 and support from the Air Force. E.P. acknowledges support from the Intel Corp. via the FEINMAN program. R.G. acknowledges

support from the National Science Foundation under Grant DMR-2102895. A.L. acknowledges support from the Army Research Laboratory as part of the Collaborative for Hierarchical Agile and Responsive Materials (CHARM) under cooperative agreement W911NF-19-2-0119. L.W.M. acknowledges support from the National Science Foundation under Grant DMR-1708615. This research used resources of the Advanced Light Source, which is a U.S. Department of Energy, Office of Science, User Facility under contract no. DE-AC02-05CH11231.

Conflict of Interest

The authors declare no conflict of interest.

Data Availability Statement

Research data are not shared.

Keywords

orbital structure, oxygen electrocatalysis, perovskite thin films, X-ray linear dichroism

Received: July 17, 2021
Revised: October 7, 2021
Published online: October 24, 2021

[1] C. Sun, R. Hui, J. Roller, *J. Solid State Electrochem.* **2010**, *14*, 1125.
[2] J. A. Kilner, M. Burriel, *Mater. Res.* **2014**, *44*, 365.
[3] S. J. Skinner, *Int. J. Inorg. Mater.* **2001**, *3*, 113.
[4] W. T. Hong, R. E. Welsch, Y. Shao-Horn, *J. Phys. Chem. C* **2015**, *120*, 78.
[5] J. Suntivich, H. A. Gasteiger, N. Yabuuchi, H. Nakanishi, J. B. Goodenough, Y. Shao-Horn, *Nat. Chem.* **2011**, *3*, 546.
[6] Y.-L. Lee, J. Kleis, J. Rossmeisl, Y. Shao-Horn, D. Morgan, *Energy Environ. Sci.* **2011**, *4*, 3966.
[7] J. Suntivich, W. T. Hong, Y.-L. Lee, J. M. Rondinelli, W. Yang, J. B. Goodenough, B. Dabrowski, J. W. Freeland, Y. Shao-Horn, *J. Phys. Chem. C* **2014**, *118*, 1856.
[8] D. N. Mueller, M. L. Machala, H. Bluhm, W. C. Chueh, *Nat. Commun.* **2015**, *6*, 6097.
[9] J. Suntivich, K. J. May, H. A. Gasteiger, J. B. Goodenough, Y. Shao-Horn, *Science* **2011**, *334*, 1383.
[10] Z. Shao, S. M. Haile, *Nature* **2004**, *431*, 170.
[11] J. Hwang, Z. Feng, N. Charles, X. R. Wang, D. Lee, K. A. Stoerzinger, S. Muy, R. R. Rao, D. Lee, R. Jacobs, D. Morgan, Y. Shao-Horn, *Mater. Today* **2019**.
[12] B. Koo, H. Kwon, Y. Kim, H. G. Seo, J. W. Han, W. Jung, *Energy Environ. Sci.* **2017**, *11*, 71.
[13] K. A. Stoerzinger, W. S. Choi, H. Jeen, H. N. Lee, Y. Shao-Horn, *J. Phys. Chem. Lett.* **2015**, *6*, 487.
[14] M. Kubicek, Z. Cai, W. Ma, B. Yildiz, H. Hutter, J. Fleig, *ACS Nano* **2013**, *7*, 3276.
[15] H. Jalili, J. W. Han, Y. Kuru, Z. Cai, B. Yildiz, *J. Phys. Chem. Lett.* **2011**, *2*, 801.
[16] J. R. Petrie, V. R. Cooper, J. W. Freeland, T. L. Meyer, Z. Zhang, D. A. Lutterman, H. N. Lee, *J. Am. Chem. Soc.* **2016**, *138*, 2488.
[17] D. Lee, R. Jacobs, Y. Jee, A. Seo, C. Sohn, A. V. Ievlev, O. S. Ovchinnikova, K. Huang, D. Morgan, H. N. Lee, *J. Phys. Chem. C* **2017**, *121*, 25651.
[18] S. A. Akhade, J. R. Kitchin, *J. Chem. Phys.* **2012**, *137*, 084703.
[19] J. E. Readman, A. Olafsen, Y. Larring, R. Blom, *J. Mater. Chem.* **2005**, *15*, 1931.
[20] R. Gao, A. Fernandez, T. Chakraborty, A. Luo, D. Pesquera, S. Das, G. Velarde, V. Thoréton, J. Kilner, T. Ishihara, S. Nemšák, E. J. Crumlin, E. Ertekin, L. W. Martin, *Adv. Mater.* **2021**, 2100977.
[21] J. A. Lane, J. A. Kilner, *Solid State Ionics* **2000**, *136–137*, 997.
[22] L. Yan, K. R. Balasubramaniam, S. Wang, H. Du, P. Salvador, *MRS Online Proc. Libr.* **2010**, *1255*, 1.
[23] L. Yan, K. R. Balasubramaniam, S. Wang, H. Du, P. A. Salvador, *Solid State Ionics* **2011**, *194*, 9.
[24] R. A. Cox-Galhotra, S. McIntosh, *Solid State Ionics* **2010**, *181*, 1429.
[25] K. Kerman, C. Ko, S. Ramanathan, *Phys. Chem. Chem. Phys.* **2012**, *14*, 11953.
[26] R. Merkle, J. Maier, *Angew. Chem., Int Ed.* **2008**, *47*, 3874.
[27] A. Aguadero, L. Fawcett, S. Taub, R. Woolley, K.-T. Wu, N. Xu, J. A. Kilner, S. J. Skinner, *J. Mater. Sci.* **2012**, *47*, 3925.
[28] M. Merz, P. Nagel, C. Pinta, A. Samartsev, H. v. Löhneysen, M. Wissinger, S. Uebe, A. Assmann, D. Fuchs, S. Schuppler, *Phys. Rev. B* **2010**, *82*, 174416.
[29] M. W. Haverkort, Z. Hu, J. C. Cezar, T. Burnus, H. Hartmann, M. Reuther, C. Zobel, T. Lorenz, A. Tanaka, N. B. Brookes, H. H. Hsieh, H.-J. Lin, C. T. Chen, L. H. Tjeng, *Phys. Rev. Lett.* **2006**, *97*, 176405.
[30] J. L. Hueso, J. P. Holgado, R. Pereñíguez, S. Mun, M. Salmeron, A. Caballero, *J. Solid State Chem.* **2010**, *183*, 27.
[31] M. Abbate, F. M. F. de Groot, J. C. Fuggle, A. Fujimori, O. Strebel, F. Lopez, M. Domke, G. Kaindl, G. A. Sawatzky, M. Takano, Y. Takeda, H. Eisaki, S. Uchida, *Phys. Rev. B* **1992**, *46*, 4511.
[32] D. Pesquera, G. Herranz, A. Barla, E. Pellegrin, F. Bondino, E. Magnano, F. Sánchez, J. Fontcuberta, *Nat. Commun.* **2012**, *3*, 1189.
[33] J. W. Freeland, J. Liu, M. Kareev, B. Gray, J. W. Kim, P. Ryan, R. Pentcheva, J. Chakhalian, *EPL-Europhys. Lett.* **2011**, *96*, 57004.
[34] A. S. Disa, F. J. Walker, S. Ismail-Beigi, C. H. Ahn, *APL Mater.* **2015**, *3*, 062303.
[35] P. C. Rogge, R. J. Green, P. Shafer, G. Fabbris, A. M. Barbour, B. M. Lefler, E. Arenholz, M. P. M. Dean, S. J. May, *Phys. Rev. B* **2018**, *98*, 201115.
[36] G. van der Laan, *J. Phys. Soc. Jpn.* **1994**, *63*, 2393.
[37] B. T. Thole, G. van der Laan, *Phys. Rev. Lett.* **1992**, *70*, 2499.
[38] A. Staykov, H. Téllez, T. Akbay, J. Druce, T. Ishihara, J. Kilner, *Chem. Mater.* **2015**, *27*, 8273.